ACS NANO
Cite This: ACS Nano 2018, 12, 10703−10711
www.acsnano.org

ARTICLE

Living Nanospear for Near-Field Optical Probing

Yuchao Li,[†] Hongbao Xin,[†] Yao Zhang,[†] Hongxiang Lei,[‡] Tianhang Zhang,[§,∥] Huapeng Ye,[∥] Juan Jose Saenz,[⊥,#] Cheng-Wei Qiu,[*,§,∥] and Baojun Li[*,†]

[†]Institute of Nanophotonics, Jinan University, Guangzhou 511443, China
[‡]School of Materials Science and Engineering, Sun Yat-Sen University, Guangzhou, 510275, China
[§]Graduate School for Integrative Sciences and Engineering, National University of Singapore, Centre for Life Sciences (CeLS), #05-01, 28 Medical Drive Singapore117456, Singapore
[∥]Department of Electrical and Computer Engineering, National University of Singapore, Singapore 117583, Singapore
[⊥]Donostia International Physics Center (DIPC), Paseo Manuel de Lardizabal 4, Donostia-San Sebastian 20018, Spain
[#]IKERBASQUE, Basque Foundation for Science, 48013 Bilbao, Spain

Supporting Information

ABSTRACT: **Optical nanoprobes, designed to emit or collect light in the close proximity of a sample, have been extensively used to sense and image at nanometer resolution. However, the available nanoprobes, constructed from artificial materials, are incompatible and invasive when interfacing with biological systems. In this work, we report a fully biocompatible nanoprobe for subwavelength probing of localized fluorescence from leukemia single-cells in human blood. The bioprobe is built on a tapered fiber tip apex by optical trapping of a yeast cell (1.4 μm radius) and a chain of *Lactobacillus acidophilus* cells (2 μm length and 200 nm radius), which act as a high-aspect-ratio nanospear. Light propagating along the bionanospear can be focused into a spot with a full width at half-maximum (fwhm) of 190 nm on the surface of single cells. Fluorescence signals are detected in real time at subwavelength spatial resolution. These noninvasive and biocompatible optical probes will find applications in imaging and manipulation of biospecimens.**

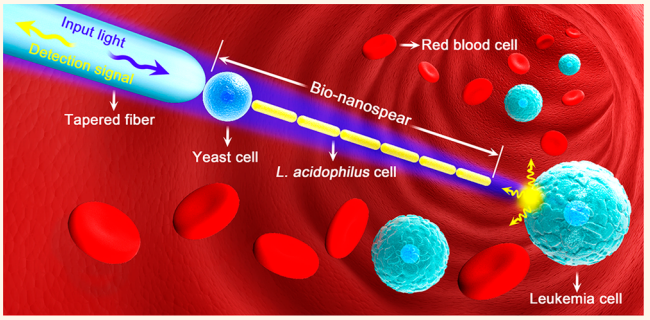

KEYWORDS: *optical trapping, subwavelength, optical probe, near field, single cells*

The past decade has witnessed an encouraging development of near-field techniques that enables surpassing of the diffraction limit, such as superlens,[1] hyperlens,[2] microsphere assisted imaging[3] and near-field scanning nano probes.[4] Because of flexibility and miniaturization, nanoprobes are regarded as a promising near-field nanotool for high-resolution imaging and sensing, and they have been extensively used in the fields of surface topography imaging,[5−7] biosensing,[8−10] nanospot-welding,[11,12] nanoparticle characteristics,[13] nanolithography,[14] optical trapping,[15−18] cellular endoscopy,[19,20] and optogenetics.[21] State-of-the-art nanoprobes are typically fabricated with lab-on-a-tip techniques, that is, by integrating nanostructures on the tip of an optical fiber, such as coating with a layer of metal nanofilm,[22] etching with plasmonic nanoantennas,[23] or attaching with a single gold nanorod,[24] semiconductor nanowire,[19] metal nanoparticle,[25] or photonic crystal nanocavity.[26] On the basis of the optical resonances of these nanostructures, the nanoprobes can concentrate the illumination light into a confined region, allowing us to probe samples with a nanometer resolution. However, these synthetic nanostructures are constructed with noble metal or semiconductor materials, which intrinsically lack biocompatibility and easily rupture the specimens when interfacing with cells. Moreover, to prepare these nanostructures, sophisticated nanofabrication processes and electrochemical reactions are often required. The quest for a biomaterial, which can be directly acquired from nature, to assemble a biocompatible and noninvasive nanoprobe is still open.

Fortunately, lessons from nature have shown that living cells are native optical materials that possess an amazing ability to manipulate light. For instance, algae cells are capable of focusing sunlight to improve the efficiency of phototaxis and photosynthesis, and so behave as microlenses.[27] Additionally, living cells in plant stems function as waveguides that can

Received: July 11, 2018
Accepted: September 28, 2018
Published: September 28, 2018

DOI: 10.1021/acsnano.8b05235
ACS Nano 2018, 12, 10703−10711

conduct certain wavelengths of light to the roots.[28] Furthermore, Müller cells in human eyes have the capacity to transmit light from the retina surface to photoreceptors, acting as optical fibers.[29] These cellular optics in nature inspire us to directly use biological cells as optical devices. Previous works have employed diatom cells, red blood cells, yeast cells, embryonic kidney cells, and *Escherichia coli* cells for integration into functionalized devices, such as force probes,[30,31] optofluidic microlenses,[32,33] biological lasers,[34] and biophotonic waveguides.[35]

In this work, we propose a living nanoprobe for near-field probing with subwavelength spatial resolution. We name this nanoprobe a bionanospear, whose "handle" is made of a tapered fiber and "head" is assembled with a yeast cell and a chain of nanosized *L. acidophilus* cells. After three steps of focusing by the tapered fiber, yeast, and *L. acidophilus* cells, respectively, the bionanospear can concentrate illumination light into a subwavelength region. Therefore, optical signals are detected in real time for near-field probing at subwavelength resolution. As a bionanophotonic application, localized fluorescence from the surface of leukemia cells was probed in human blood. The bionanospear is flexible and deformable with less chance to puncture and damage the living specimens under measurement, thus it can be used as a noninvasive tool for near-field imaging and sensing of biosamples.

RESULTS

Figure 1 panels a to c schematically show the experimental process (see Supplementary Video). First, human blood sample carrying leukemia cells was injected into a mixture of yeast and *L. acidophilus* cells (Figure 1a). Then, a tapered fiber (Figure 1d), which can be used to trap cells, guide light, and collect optical signals, was inserted into the cell medium using a tunable micromanipulator (Figure 1b, see experimental setup in Figure S1). An 808 nm laser beam with an optical power of 15 mW, which exhibits low absorption by biological specimens[36] was launched into the taper fiber to create a stable optical trap. By precisely moving the tapered fiber to approach a yeast cell (Figure 1e), the yeast cell could be captured at the tip of the tapered fiber by the optical gradient force. Benefiting from the spherical shape of the yeast, the trapping laser beam could be focused into a tiny region and exert a strong optical force on a *L. acidophilus* cell (Figure 1f) that traps it behind the yeast. The trapped *L. acidophilus* cell automatically aligned its long axis along the optical axis as this was the stable orientation (see simulated explanation in Figure S2). With this alignment, the trapping laser beam could propagate through the *L. acidophilus* cell and exert an optical force on other *L. acidophilus* cells, which were orderly bound together by an optical binding effect,[37,38] and finally formed the bionanospear. The optical forces F of the cells in the bionanospear can be measured by $F = \kappa q$ (1), where κ represents the trapping stiffness and q is the positional coordinate of the cells. Therefore, determination of κ is of importance to the optical force measurement. The trapping stiffness κ of the bionanospear can be calculated by tracking the Brownian fluctuations of the cells (at a trapping power of 15 mW) with high-speed video microscopy.[39] As a result, the values of κ for the yeast cell and six *L. acidophilus* cells in the y direction were measured as 4.3, 9.5, 12.3, 11.5, 9.5, 8.4, and 7.8 × 10^{-2} pN/nm, respectively (Figure S3). Alternatively, κ can also be obtained by using the backscattered light at 808 nm to perform a frequency-domain analysis of the thermal fluctuations of the cells. Here, we performed the analysis for the yeast cell as an example (Figure S4). The result shows that κ of the yeast cell is 4.1 × 10^{-2} pN/nm, which agrees with the value of 4.3 × 10^{-2} pN/nm measured by the video tracking method. After the determination of κ, the optical force F can be obtained from eq (1), which varies from the positional coordinates of the cells. By means of the precise manipulation, the formed bionanospear can guide an input light to designated positions and detect optical signals from biological cells, such as single leukemia cells in human blood (Figure 1c). The bionanospear is biocompatible and environmental friendly. After use, the bionanospear can be left in biological systems without extra processing, as the yeast and *L. acidophilus* cells natively exist in human body to provide health benefits.

Figure 1g shows a formed bionanospear assembled with a yeast and five *L. acidophilus* cells. The length of the bionanospear can be adjusted in real-time by trapping different numbers of cells, enabling self-adapting to different biological environments, while the length of conventional optical nanoprobes is predesigned and unadjustable. In the trapping process, two methods were applied to precisely control the numbers of the cells. First, the cells could be orderly trapped one by one through manipulation of the optical fiber probe at a high precision (50 nm). Second, the number of the trapped cells could be controlled by the microscopic observation with a high-numerical-aperture objective, and by monitoring the backscattering signal of the trapped cells with a fiber photodetector that was connected to the tapered fiber. The size of the nanospear is mainly limited by the optical power of the optical trapping laser. The maximum size of the nanospear was approximately 120 μm in length with the optical power of 200 mW launching into the spear. In our experiments, the optical power was set to less than 200 mW because higher optical powers will damage the trapped cells and induce the thermal convection in the liquid medium. After assembly of the bionanospear, the 808 nm trapping laser remained on, and then a visible illumination light was launched into the bionanospear by a fiber coupler. The illumination light propagating along the tapered fiber was coupled into the yeast, then focused into the *L. acidophilus* cells and transmitted along the cell chain, and finally emitted a tiny light spot at the bionanospear tip (Figure 1h–j). Here, the bionanospear can function as a waveguide because the refractive index of cells (n_{cell} = 1.40)[40] is larger than that of water (n_{water} = 1.33). The refractive index contrast can be calculated as $\Delta = (n_{cell}^2 - n_{water}^2)/2n_{cell}^2$ = 4.9%. Additional simulations and calculations demonstrate that the evanescent field of the propagating light through the bionanospear is narrower than that of bare tapered fibers with a subwavelength end-tip (see details in Figure S5). This is mainly because the cell chain in the bionanospear has a periodic refractive index distribution and hemispherical caps, which can repeatedly focus the propagating light while reducing the divergent light. Therefore, the evanescent field outside the cell chain can be effectively suppressed, which allows the subwavelength light confinement with a low index contrast. Line intensity profiles (insets of Figure 1h–j) in the vertical direction reveal the fwhm of the output light spots were 345, 282, and 248 nm for the illumination wavelengths of 644, 532, and 473 nm, respectively. To further confirm the light-guiding ability of the cell chain with the output light spots, a controlled experiment and simulation was performed to record the scatter spot of a single *L. acidophilus* cell, which was located at the same position as the last cell of the cell chain (Figure S6). The experiment and simulation show that the optical intensity of the light spot from the cell chain is

DOI: 10.1021/acsnano.8b05235
ACS Nano 2018, 12, 10703–10711

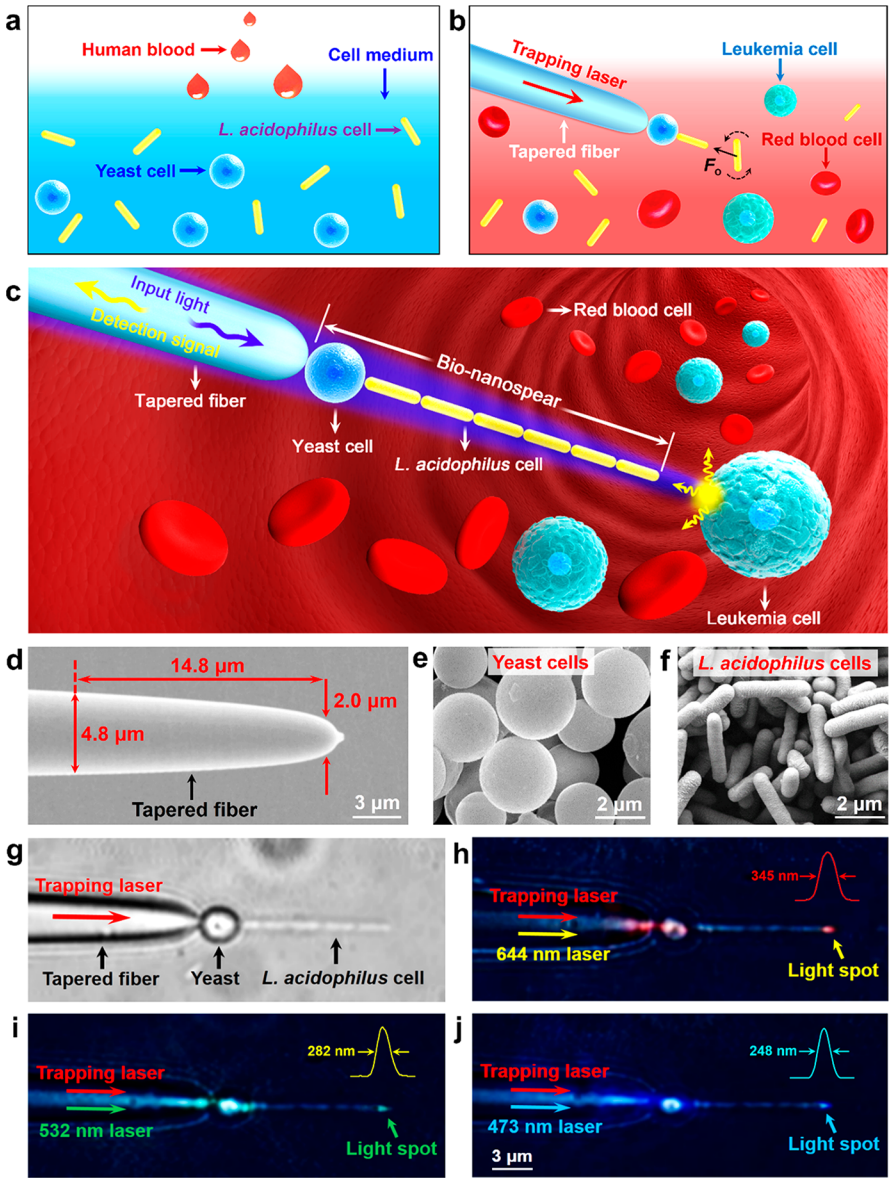

Figure 1. Optical assembly and light propagation of the bionanospear. (a–c) Schematic illustration shows the assembly process of the bionanospear. (d) Scanning electron microscope (SEM) image of the tapered fiber with a diameter in the taper tip of 2.0 μm. (e) SEM image showing yeast cells have smooth surfaces and spherical shapes with a radius of 1.0 ± 0.4 μm. (f) SEM image of *L. acidophilus* cells that have nanocapsule-like shapes with a radius of 200 ± 10 nm and length of 2.0 ± 0.7 μm. (g) Optical image of a bionanospear assembled with a yeast and five *L. acidophilus* cells. (h–j) Dark-field images show a 644 nm red light (h), 532 nm green light (i), and 473 nm blue light (j) propagating through the bionanospear and being focused into subwavelength light spots at the end of the bionanospear. Insets are the line intensity profiles through the focuses of the light spots in the lateral direction for each image.

approximately three times higher than that of the single cell without the cell chain, which is attributed to the light guiding and focusing by the cell chain. Additional experiments and simulations were performed to characterize how the spot size changes with the number of *L. acidophilus* cells and the chain length (see details in Figure S7). The experimental results show that the light spot size of the illumination light at 532 nm wavelength, for example, varies from 282 to 340 nm when the number of *L. acidophilus* cells ranges from 1 to 13 (chain length: 2 to 29 μm), which agrees with the simulation results. It is worth noting that the monotonic trend in spot size is resulted from the photonic nanojet-induced mode of the propagating light in the cell chain. Previous works have verified that the periodically focused and diverged effect of the photonic nanojet-induced mode can cause a nonmonotonic trend in spot size from a microlens chain.[41,42] Similarly, this effect also exists in the cell chain since each cell in the chain can be regarded as a microlens. Because of this effect, the minimum spot size of the cell chain will occur at the cells located in the light focusing region (i.e., ~5 and 11 cells in the nanospear). For the applications of single-cell probing and imaging, the light spot size of the nanospear is important because it determines the spatial resolution of the optical signals. In terms of the light spot size, the optimized result is five *L. acidophilus* cells, as indicated in Figure S7g. Therefore, we used the nanospear with five *L. acidophilus* cells to detect a fluorescence signal from nanoparticles and single cells in the following experiments.

The resolution of the bionanospear was determined by resolving the fluorescence spot from a polystyrene (PS)

DOI: 10.1021/acsnano.8b05235
ACS Nano 2018, 12, 10703–10711

nanoparticle dimer. The nanoparticles with a diameter of 120 nm were stably assembled on a glass substrate *via* carboxylate surface functionalization.[43] The chemical binding force between the nanoparticles and substrate was much stronger than the optical force, so that the nanoparticles could not be trapped by the nanospear. To excite the nanoparticles, a diode laser with a wavelength of 390 nm was launched into the bionanospear. The distance between the nanospear and the dimer was controlled by monitoring the backscattering signal of the 808 nm trapping laser and meanwhile looking at the microscope image. The control procedure is as follows. First, the nanospear was coarsely manipulated to approach the dimer with large steps (500 nm per step) under the observation of the microscope. Then, the position of the nanospear was finely adjusted with smaller steps (50 nm per step) until the backscattering signal reaches the predetermined threshold value, where the position of the nanospear was set as the starting point to scan. Finally, the bionanospear was scanned with 50 nm step across the nanoparticle dimer in the lateral direction. The fluorescence spots from the dimer at each scanning pixel point were detected on a charge-coupled device (CCD) through an objective lens, as schematically and experimentally shown in Figure 2a,b. The intensity of fluorescence spots was measured by performing three-dimensional color mapping using MATLAB software. To reduce the influence of the Brownian fluctuation on the bionanospear, the nanoparticle dimer was repeatedly scanned three times in both the forward and reverse directions. Then the average values and standard deviations of the fluorescence intensity obtained from the three repeated experiments were recorded versus the positions of the bionanospear (indicated as black dots in Figure 2c). Insets of Figure 2c show the images of the fluorescence spots when the vertical distances between the bionanospear tip and the dimer center are 110 nm (I), 0 nm (II), and −110 nm (III). The intensity−distance profile can be fitted with bi-Gaussian model (indicated as blue line in Figure 2c). The peak−valley ratio of the bi-Gaussian fitting is 37%, which is larger than 20% defined in the standard Rayleigh's criterion for distinguishing two adjacent spots in an image.[44] Moreover, the peak-to-peak distance indicates that the center-to-center distance of the nanoparticle dimer is 220 nm, which shows a resolution discrepancy of 15 nm from the value (235 nm) obtained from the SEM observation (Figure 2d). The fluorescence resolution could change with the power of the trapping laser. For example, the values of the fluorescence resolution were 262, 254, 218, 220, and 248 nm when the trapping powers were set as 5, 10, 12, 15, and 20 mW, respectively (Figure S8a). The corresponding resolution discrepancies $|\Delta R|$ between the fluorescence resolution R_{fluo} and actual resolution R_{SEM} (235 nm) obtained by the SEM image were 27, 19, 17, 15, and 13 nm, respectively. It can be seen that the resolution discrepancy $|\Delta R|$ was reduced by increasing the trapping powers, because the Brownian fluctuations of the optically bound *L. acidophilus* cells can be suppressed with higher optical powers. By looking at the illumination light scattered by the nanospear end with the video tracking method, the optically bound particle motion can be tracked in time. Then by fitting Gaussian models to the positions distributions of the real-time tracks, the lateral Brownian fluctuations σ of the nanospear end can be recorded as 13.6, 9.2, 8.1, 7.3, and 6.4 nm for the trapping powers of 5, 10, 12, 15, and 20 mW, respectively. From the comparison of the Brownian fluctuations σ and the resolution discrepancies $|\Delta R|$ (Figure S8b), it can be found that the values of 2σ approximately equal to $|\Delta R|$. Therefore, the measured fluorescence resolution R_{fluo} can be corrected by $R_{fluo} = R_{SEM} \pm 2\sigma$. For comparison, when the nanoparticle dimer was imaged with a conventional fluorescence microscope, the fluorescence spot from the dimer was nearly overlapped and could not be resolved at all (Figure 2e). This experiment indicates that the bionanospear can be used for near-field scanning imaging with a subwavelength spatial resolution. Compared with other near-field imaging approaches, the spatial resolution of the nanospear is higher than that of subwavelength metalenses (450 nm),[45] and similar to that of nanoscale spherical lenses (220 nm).[46] When compared with far-field super-resolution approaches, such as direct stochastic optical reconstruction microscopy (dSTORM) and superoscillatory lenses with spatial resolutions of 20 and 105 nm,[47,48] respectively, the resolution of the nanospear is relatively low because of the Brownian motion and small refractive index of the trapped cells. However, the spatial resolution of the nanospear can be further improved by trapping other cells with larger refractive index, such as diatom cells, or using higher trapping power to suppress the Brownian motion of the nanospear.

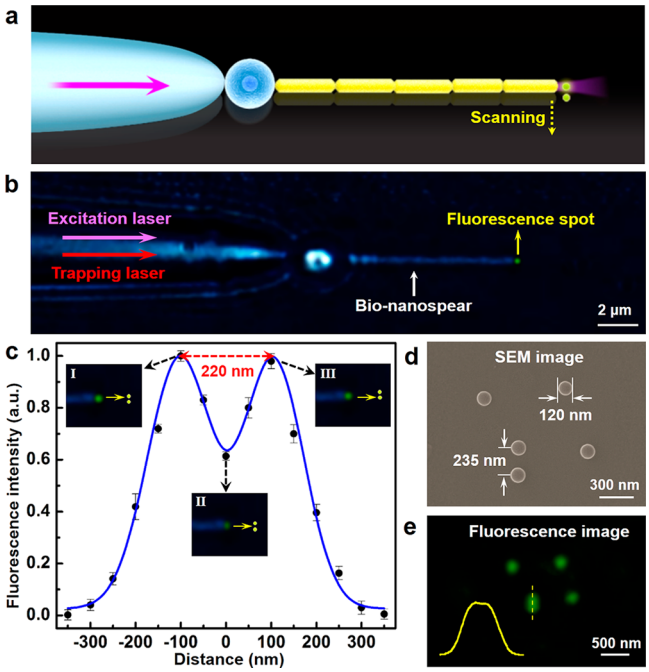

Figure 2. Optical resolution of the bionanospear. (a,b) Schematic illustration (a) and dark-field image (b) showing the bionanospear was scanned (50 nm per step) across the nanoparticle dimer and the fluorescence spot from the dimer was recorded on a CCD through an objective lens. (c) Intensity of the fluorescence spot versus the position of the bionanospear with a bi-Gaussian fitting. The black dots denote the experimental data, and blue line indicates the bi-Gaussian fitting. The peak−valley ratio from the bi-Gaussian fitting is 37% and the peak-to-peak distance is 220 nm. Insets showing the images of the fluorescence spots when the vertical distances between the bionanospear tip and the dimer center are 110 nm (I), 0 nm (II), and −110 nm (III). (d) SEM image showing the diameter of the nanoparticles is 120 nm and the center-to-center distance is 235 nm. (e) Fluorescence image of the nanoparticle dimer with wide-field excitation of a conventional fluorescence microscope. The inset shows the line intensity profile through the center of the fluorescence spot from the nanoparticle dimer.

As a potential application, the bionanospear was used to probe the localized fluorescence of leukemia cells in human

DOI: 10.1021/acsnano.8b05235
ACS Nano 2018, 12, 10703−10711

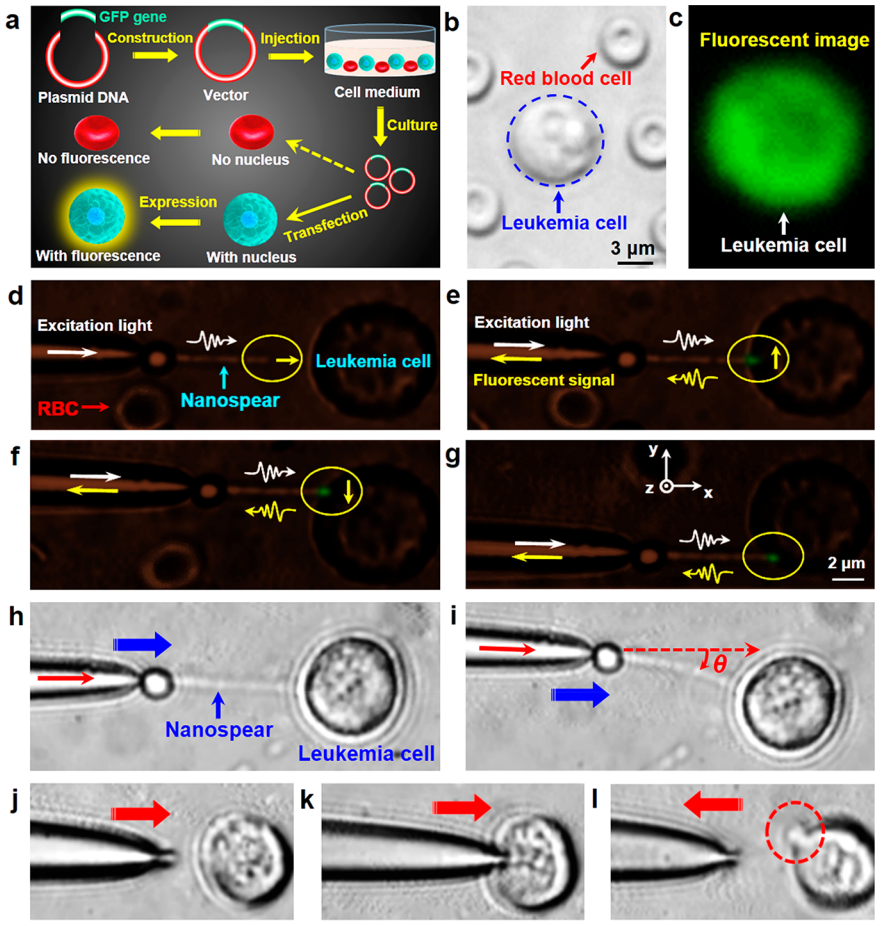

Figure 3. Single-cell probing. (a) GFP transfection process. (b) Bright-field optical image of a mixture of human red blood cells and GFP leukemia cells (labeled with a blue circle). (c) Corresponding fluorescence image shows the green fluorescent light of the leukemia cells. (d–g) Excitation and detection of local fluorescence from a leukemia cell in human blood by manipulating the bionanospear to scan the cell. Dark-field optical image of panel d shows the bionanospear separated with a 3-μm gap in the x direction from the leukemia cell. By moving the bionanospear in the x (e), + y (f), and −y (g) directions to contact with the leukemia cell, different points on the surface of the leukemia cell were excited and the green fluorescence was detected. (h,i) Flexibility testing by pushing the bionanospear against the cell membrane of a leukemia cell (h), and then the bionanospear was bent with a bending angle θ of 15° (i). (j–l) An optical fiber probe with a submicrometer tip was forced against the leukemia cell (j), showing the fiber probe could puncture into the cell (k), and cause a hole in the cell membrane after pulling out the fiber (l).

blood. The leukemia cells were selectively stained with green fluorescent protein (GFP) by adding plasmid-GFP vectors into the cell culture medium that contained the leukemia cells and red blood cells (Figure 3a). Therefore, the leukemia cells could emit the fluorescence under the wide-field excitation with a fluorescence microscope (Figure 3b,c). The fluorescent image of the leukemia cell shows that the whole cell, including the top and bottom surfaces, was excited owing to the large excitation area of the fluorescence microscope. In this case, out-of-focus fluorescence noise could enter the focal plane of the objective lens and blurred the details of the in-focus image.[49] Moreover, this fluorescence image presents a relatively low resolution. With assistance of the bionanospear, the output light was closely confined in near field, offering a much smaller excitation volume that could excite a subwavelength spot on the cellular surface with much lower background noise and higher resolution. Figure 3 panels d to g show the spot excitation capability by manipulating the bionanospear to approach the cell membrane. The dark-field image shows that no fluorescence was detected when the bionanospear was separated horizontally by 3 μm from the surface of a leukemia cell (Figure 3d). Once the bionanospear contacted closely with the cell membrane, a distinct fluorescent spot was observed (Figure 3e). By precisely moving the bionanospear to scan the cell surface, other locations on the cell surface were also excited and the fluorescent spots were detected (Figure 3f,g). It is worth noting that the backscattering signal of the 808 nm trapping laser was monitored in real time to avoid trapping other cells and objects during the measurements. When other cells and objects approach the nanospear, the intensity of the backscattering signal will increase abruptly. To further investigate the scanning capabilities of the nanospear, we have applied this scanning approach to a simulated blood capillary system, which was composed of a polymer microcapillary (inner diameter, 15 μm; length, 1.0 cm) and a micropump system (KDS LEGATO 270). The experimental result shows that the nanospear can be used to scan and detect a single fluorescent cancer cell in the microcapillary with a microfluidic flow at speed of 35 μm/s (see experimental details in Figure S9). Although the detection of the transgenic fluorescent cells can also be accomplished by other techniques, such as fluorescence microscope, flow cytometer, and confocal microscopy, it should be addressed that the nanospear has its superiority. For example, the subwavelength spatial resolution enables the

DOI: 10.1021/acsnano.8b05235
ACS Nano 2018, 12, 10703–10711

nanoprobe to acquire localized fluorescence from the transgenic fluorescent cells. In contrast, the fluorescence microscope or flow cytometer were commonly applied to detect the total fluorescence from the whole cells; thus, the localized details were easily obscured in the background noise. The resolution of the bionanospear is similar to that of confocal microscopy. However, thanks to its compact and miniaturized structure, the bionanospear can access some narrow environments such as biological capillaries, microfluidic channels, and lab-on-a-chip devices that are inaccessible for the confocal microscopy, functioning as a biocompatible and noninvasive endoscopy for single-cell probing and imaging. Besides, the additional uncertainty in localization of the nanospear can be suppressed by increasing the optical trapping power, because higher trapping power can exert larger optical forces and trapping stiffness on the nanospear. Although the nanospear is constructed with soft materials, it can remain stable during measurements with a scanning speed of 20 μm/s. Therefore, it is reasonable to implement measurements (*e.g.*, fluorescence or backscattering signals) on a conventional scanning probe microscope with the biological nanoprobe. To demonstrate this, a preliminary experiment demonstrates that the nanospear can be applied for combining fluorescence with a morphological scanning (see details in Figure S10). By using the nanospear to scan the sample (here, a fluorescent polystyrene microbead was used), the localized fluorescence from the surface of the sample was excited and detected at different positions. Then the positional coordinates of the fluorescence spots were orderly recorded as pixel points. Finally, a two-dimensional surface morphology of the sample can be reconstructed in postprocessing by superimposing all the pixel points in an image. To demonstrate the manipulation ability of the nanospear, a biospecimen (*Staphylococcus aureus*) dyed with green fluorescent protein was first trapped at the tip of the nanospear by the optical gradient force, and then manipulated to a desired position by moving the nanospear with an average speed of 26 μm/s in the x and y directions (Figure S11). This preliminary experimental example indicates that the nanospear assembled with soft materials can also find applications in the manipulation of biospecimens.

An additional experiment verified that the bionanospears are flexible and deformable when interacting with biospecimens. As shown in Figure 3h,i, the bionanospear was forced against a leukemia cell, then the bionanospear was bent to an angle θ of 15° without puncture to the cell membrane. This occurred because the bionanospear exerts a gentle optical force (scale of 10^{-11} N) instead of a mechanical force on the biosamples. A certain degree of the deformability of the nanospear has no obvious influence on the scanning capabilities. Simulation results show that, even if the deformation angle of the nanospear increases from 15 to 45 deg, the incident light can still effectively propagate along the nanospear and emit a subwavelength light spot at the tip (see details in Figure S12). For comparison, a fiber probe with a submicrometer tip, which is commonly used in scanning probe microscopes, was also used by pushing it against the leukemia cell (Figure 3j). As a result of the relatively large dimension and rigid structure, the fiber probe could easily insert into the cell (Figure 3k), and rupture the cell membrane (Figure 3l). For this reason, commercial scanning probe microscopes require additional feedback control system to ensure a precise distance between the probe and samples, especially for soft materials. One main concern about the bionanospears is the photodamage to the cells by the input lasers. To test the cell viability, a 0.4% trypan blue dye (Solarbio) was injected into the cell suspension with a volume ratio of 1:9 after the experiments. The results showed that the cells were not stained blue, which indicated that the cells were alive. To further investigate the effect of light propagation through the cells, an additional experiment was performed. In this experiment, the nanospear was exposed to trapping light with an optical power of 15 mW for about 3 h. During this process, the *L. acidophilus* cells in the nanospear could keep on growing and dividing. The average division time of the *L. acidophilus* cells was measured as approximately 1 h, which was similar to the division time of other cells out of the trap and away from the light irradiation. This experiment indicates that light propagation has no serious effect on the functional state of the cells. Moreover, the reliability, durability and ease of the technique are important for biological applications. For a static liquid environment, as shown in the Supplemental Video, the nanospear could be easily assembled by manipulating the fiber probe to trap the cells, and on an average only one attempt was needed to get it working. Besides, the nanospear could remain stable when repeatedly imaging and measuring the same structure for over 3 h with a trapping power of 15 mW and a scanning speed of 20 μm/s. The duration can be further extended by increasing the optical power, because the trapping stiffness was proportional to the power.[50] While for a microfluidic environment, such as a microcapillary with a flow, more time (average 3 attempts) should be used to get the nanospear working mainly because of the drag force induced by the flow. However, the drag force can be easily offset by increasing the optical trapping power. For example, with a higher optical trapping power (30 mW), the nanospear could be flexibly manipulated in a microfluid with a flow velocity of 35 μm/s (Figure S9).

To investigate the light propagation and trapping stability of the bionanospear, a theoretical model was built with a finite element method using COMSOL Multiphysics (see Methods). Figure 4a shows the simulated energy density distribution of the 808 nm trapping laser beam output from a bare tapered fiber. The laser beam was prefocused by the tapered fiber with a distance of 3 μm in the x direction between the focus and the tapered fiber. When a yeast was positioned at the tapered fiber tip, a subwavelength focused beam was generated (Figure 4b), which resulted from interferences between the field scattered by the yeast cell and the large angular components of the incident Gaussian beam passing aside the cell. Then the focus spot was further enhanced and concentrated in the near-field by horizontally placing a *L. acidophilus* cell behind the yeast (Figure 4c). Line scans were performed through the focal planes in Figure 4a–c in the y direction, and the results show that the fwhm of the output light spots generated by the tapered fiber, yeast, and *L. acidophilus* cell were 1.1 μm, 480 nm, and 430 nm, respectively (Figure 4d). By connecting more *L. acidophilus* cells, the input light could propagate along the bionanospear, and emit a subwavelength light spot in the near-field near the bionanospear tip (Figure 4e–g). The energy density profiles (Figure 4h) show that the fwhm of the light spots was calculated to be 200, 240, 280, 340, and 430 nm for input wavelengths of 390, 473, 532, 644, and 808 nm, respectively, which agreed with the experimental observations. The optical force (F_0) and trapping potential (U) exerted on the yeast and *L. acidophilus* cells was calculated using the time-independent Maxwell stress tensor (Figure S13 and Figure 4i). The results show that the maximum F_0 exerted on the yeast and *L. acidophilus*

DOI: 10.1021/acsnano.8b05235
ACS Nano 2018, 12, 10703–10711

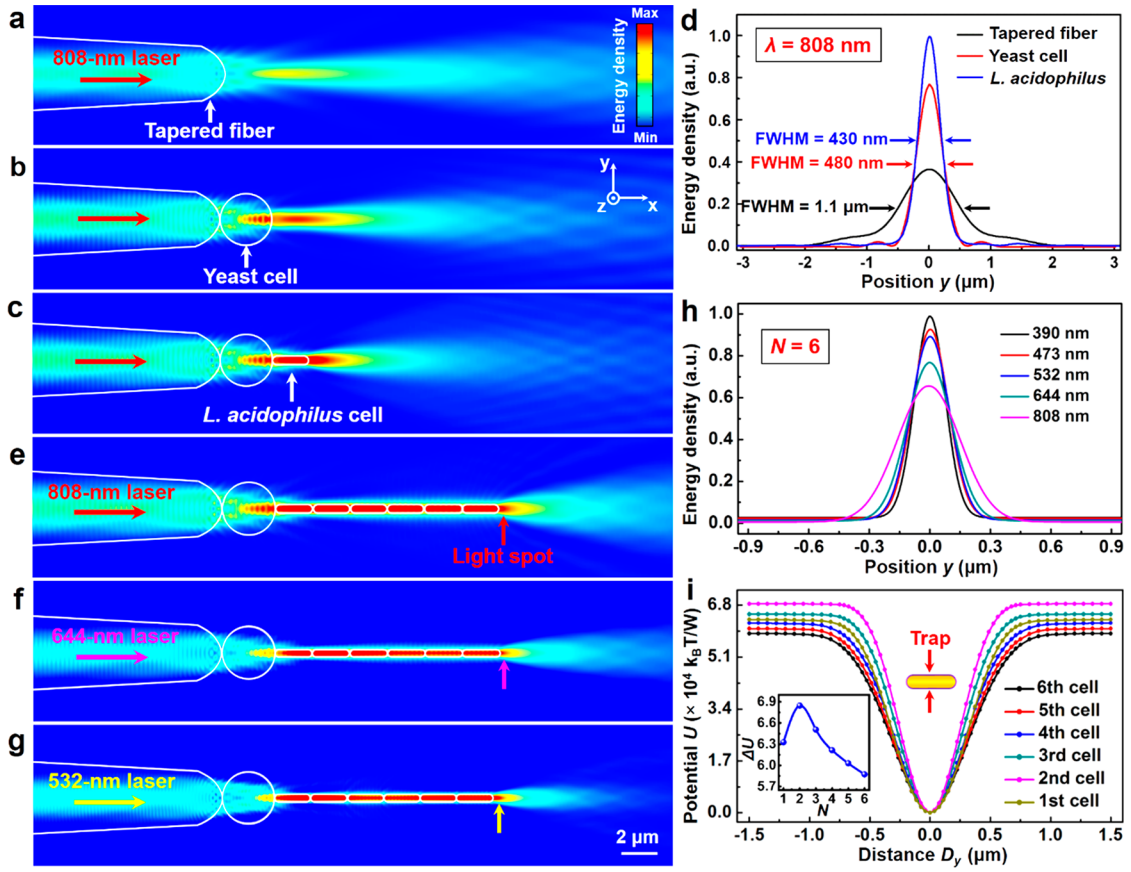

Figure 4. Numerical simulation and calculation. (a) Energy density distribution output from a bare tapered fiber in the *x*-*y* plane. (b) The 808 nm laser is focused into a subwavelength light spot by positioning a spherical yeast cell at the end of the tapered fiber. (c) The light spot is further concentrated with a *L. acidophilus* cell. (d) Normalized energy density profiles at the focal planes of the output light spots in panels a to c in the *y* direction. (e–g) Energy density distributions of the 808 nm (e), 644 nm (f), and 532 nm (g) laser beam propagating along the bionanospear with an *L. acidophilus* cell number *N* of 6 and emitting tiny light spots in the end. (h) Energy density profiles at the focal planes of the output light spots of the bionanospear in the *y* direction with different input wavelengths for *N* = 6. (i) Simulated potential *U* of each *L. acidophilus* cell in the bionanospear as a function of distance D_y. The inset shows the potential depth ΔU as a function of the number *N* of the attached *L. acidophilus* cells (first to sixth).

cells were 790 and 660 pN/W, respectively, and the potential depth ΔU of the yeast and each *L. acidophilus* cell were calculated as 23, 6.3, 6.8, 6.5, 6.2, 6.0, and 5.9 × 10^4 k_BT/W, respectively. The inset of Figure 4i depicts the tendency of the potential depth ΔU as a function of the number *N* of the attached *L. acidophilus* cells (first to sixth). It can be seen that the value of ΔU reaches the maximum at $N = 2$, and then it generally decreases when $N > 2$. This tendency results from the competition between the light focusing and optical loss of the *L. acidophilus* cell chain. Additional calculations demonstrate that the optical intensity along the *L. acidophilus* cell chain reaches the maximum at the second *L. acidophilus* cell and then slightly reduces for the increasing cell number (Figure S14), which agrees with the tendency of the potential depth. Additionally, Ashkin *et al.* have verified that a stable trap requires a ΔU of about 10 k_BT to suppress the Brownian motion.[51] For the optical power of 15 mW used in our experiments, the corresponding ΔU were calculated to be 345, 95, 102, 98, 93, 90, and 89 k_BT, which were larger than 10 k_BT, indicating that the bionanospear was stable.

CONCLUSIONS

We developed a living nanoprobe, namely, a bionanospear by trapping a yeast cell and a chain of *L. acidophilus* cells at the tip of a tapered fiber probe. As a benefit of the light focusing ability of the cells, the bionanospear can deliver excitation light with a 190 nm spot size to biological samples. Optical signals are detected in real time for near-field probing at subwavelength resolution. The precise manipulation of the bionanospear allows us to probe the localized fluorescence from the surface of single leukemia cells in human blood. With the advantages of its high resolution and biocompatibility, the developed nanospear is envisioned to find relevant applications in the fields of biosensing and imaging.

METHODS

Fabrication of the Tapered Fiber. The tapered fiber was fabricated with a flame-heating technique from a multimode optical fiber (Corning Inc.). The buffer and polymer jacket of the fiber were stripped off by a fiber stripper to obtain a bare fiber of 2.5 cm in length. Before being heated, the fiber was sheathed with a glass capillary to ensure the stability of the fiber. The bare fiber outside the capillary was heated by the outer flame of an alcohol lamp at approximately 500 °C for 40 s until it reached its melting point. Then, the fiber was drawn through a heating zone of approximately 4 mm at a rate of ~3 mm/s, which then gradually tapered off, with its diameter decreasing from 125 to 10 μm with a length of ~2.0 mm. Finally, the drawing rate was increased up to ~15 mm/s until the fiber was broken with a tapered tip.

DOI: 10.1021/acsnano.8b05235
ACS Nano 2018, 12, 10703–10711

Preparation of the Mixture of the Yeast and *L. acidophilus* Cells. The yeast (*Saccharomyces cerevisiae*) and *L. acidophilus* cells (Shanghai Ruichu Biotech Co., Ltd.) were grown at room temperature in lysogeny broth for 48 h. The yeast cells were selected at the early growth stage before forming the bacterial spores, because in this stage, the yeast cells have regular shapes. The yeast cells and *L. acidophilus* cells were then washed and diluted with phosphate-buffered saline to obtain a suitable concentration of approximately 6.0×10^4 cells per microliter. Finally, they were mixed together with a volume ratio of ~1:10.

Preparation of the Mixture of the Human Blood and Leukemia Cells. Human blood (1 mL) was extracted from the fingertip of a healthy adult and then diluted with 4 mL of phosphate-buffered saline (pH = 7.44), which contained 121.5 mM NaCl, 25.2 mM Na_2HPO_4, and 4.8 mM KH_2PO_4. The leukemia cells (Zhong Qiao Xin Zhou Biotechnology Co., Ltd.) were grown in DMEM supplemented with 10% fetal bovine serum and incubated at 37 °C in 5% CO_2 overnight to obtain a concentration of ~3.0×10^4 cells per microliter. The human blood and leukemia cells suspension were mixed together with a volume ratio of ~1:5.

Transfection Process of GFP. First, lentiviral vectors (Zhong Qiao Xin Zhou Biotechnology Co., Ltd.) were constructed by linking GFP genes (10 μg) with plasmid DNA fragments (10 μg). Second, 2.5 μg of vectors and 0.5 μL of Lipofectamine 2000 reagent (Invitrogen) were diluted in 125 μL of Opti-MEM medium and then incubated for 5 min at room temperature. Third, the vectors-lipid complex was added to the mixture of the human blood and leukemia cells (final concentration: ~1 μg vectors/1 × 10^5 cells). After incubating for 48 h at 37 °C in 5% CO_2, the vectors were transfected into the leukemia cells and expressed the fluorescent proteins. The transfected cells were visualized with a fluorescence microscope (IX71, OLYMPUS).

Numerical Simulations and Calculations. The simulations were performed by COMSOL Multiphysics 4.4 with the radio frequency module (electromagnetic wave, frequency domain) and perfectly matched layer boundary conditions. The lights directed into the tapered fiber were set as unpolarized Gaussian beams. The yeast and *L. acidophilus* cell were assumed to be a dielectric sphere (radius, 1.4 μm) and nanocapsule (length, 2.0 μm; radius, 200 nm) with hemispherical caps, respectively. The mesh sizes of the regions of the tapered fiber, *L. acidophilus* cells, yeast cell, and water were set as 60, 50, 30, and 80 nm, respectively, and the corresponding refractive indices were set as 1.45, 1.40, 1.39, and 1.33, respectively.

ASSOCIATED CONTENT

Supporting Information

The Supporting Information is available free of charge on the ACS Publications website at DOI: 10.1021/acsnano.8b05235.

Theoretical details of the optical orientation, light propagation, output light spots, optical intensity and optical forces of the nanospears; experimental details of the optical setup, optical forces, light spot sizes, fluorescence resolution and single-cell scanning(PDF)

Video showing the nanobiospear assembly and light propagation (AVI)

AUTHOR INFORMATION

Corresponding Authors

*E-mail: baojunli@jnu.edu.cn.
*E-mail: eleqc@nus.edu.sg.

ORCID

Yuchao Li: 0000-0002-8436-1342
Tianhang Zhang: 0000-0002-7939-5302
Juan Jose Saenz: 0000-0002-1411-5648
Cheng-Wei Qiu: 0000-0002-6605-500X

Author Contributions

Y.L. and B.L. conceived and designed the research; Y.L. performed the experiments; Y.Z., H.L., and B.L. supported the experiments. Y.L., H.X., H.Y., J.S., C.W.Q., and B.L. analyzed the data; Y.L., H.X., and T.Z. carried out the theoretical modeling and calculations; Y.L., J.S., C.W.Q., and B.L. wrote the paper. B.L. supervised the project. All authors discussed the results.

Notes

The authors declare no competing financial interest.

ACKNOWLEDGMENTS

This work was supported by the National Natural Science Foundation of China (Nos. 61827822, 11874183, and 11774135). C.W.Q. would like to acknowledge the support from Ministry of Education, Singapore (Grant Number: R-263-000-D11-114). We thank Yingbin Huang from Zhongshan School of Medicine, Sun Yat-Sen University for experimental assistance, and Xianguang Yang from Institute of Nanophotonics, Jinan University and Caiyan Zheng from Guangzhou Red Cross Hospital for helpful discussions.

REFERENCES

(1) Kawata, S.; Inouye, Y.; Verma, P. Plasmonics for Near-Field Nano-Imaging and Superlensing. *Nat. Photonics* **2009**, *3*, 388−394.
(2) Lu, D.; Liu, Z. Hyperlenses and Metalenses for Far-Field Super-Resolution Imaging. *Nat. Commun.* **2012**, *3*, 1205.
(3) Wang, Z.; Guo, W.; Li, L.; Luk'yanchuk, B.; Khan, A.; Liu, Z.; Chen, Z.; Hong, M. Optical Virtual Imaging at 50 nm Lateral Resolution with a White-Light Nanoscope. *Nat. Commun.* **2011**, *2*, 218.
(4) Nakayama, Y.; Pauzauskie, P. J.; Radenovic, A.; Onorato, R. M.; Saykally, R. J.; Liphardt, J.; Yang, P. Tunable Nanowire Nonlinear Optical Probe. *Nature* **2007**, *447*, 1098−1101.
(5) Zhang, W.; Fang, Z.; Zhu, X. Near-field Raman Spectroscopy with Aperture Tips. *Chem. Rev.* **2017**, *117*, 5095−5109.
(6) Alù, A.; Engheta, N. Cloaked Near-Field Scanning Optical Microscope Tip for Noninvasive Near-Field Imaging. *Phys. Rev. Lett.* **2010**, *105*, 263906.
(7) Phillips, D. B.; Padgett, M. J.; Hanna, S.; Ho, Y. L.; Carberry, D. M.; Miles, M. J.; Simpson, S. H. Shape-Induced Force Fields in Optical Trapping. *Nat. Photonics* **2014**, *8*, 400−405.
(8) Zheng, X. T.; Li, C. M. Single Cell Analysis at the Nanoscale. *Chem. Soc. Rev.* **2012**, *41*, 2061−2071.
(9) Gao, Y.; Longenbach, T.; Vitol, E. A.; Orynbayeva, Z.; Friedman, G.; Gogotsi, Y. One-Dimensional Nanoprobes for Single-Cell Studies. *Nanomedicine* **2014**, *9*, 153−168.
(10) Vo-Dinh, T.; Alarie, J. P.; Cullum, B. M.; Griffin, G. D. Antibody-Based Nanoprobe for Measurement of a Fluorescent Analyte in a Single Cell. *Nat. Biotechnol.* **2000**, *18*, 764−767.
(11) Cui, J.; Yang, L.; Wang, Y.; Mei, X.; Wang, W.; Hou, C. Nanospot Soldering Polystyrene Nanoparticles with an Optical Fiber Probe Laser Irradiating a Metallic AFM Probe Based on the Near-Field Enhancement Effect. *ACS Appl. Mater. Interfaces* **2015**, *7*, 2294−2300.
(12) Yang, L.; Cui, J.; Wang, Y.; Hou, C.; Xie, H.; Mei, X.; Wang, W.; Wang, K. Nanospot Welding of Carbon Nanotubes using Near-Field Enhancement Effect of AFM Probe Irradiated by Optical Fiber Probe Laser. *RSC Adv.* **2015**, *5*, 56677−56685.
(13) Cui, J.; Zhang, J.; Wang, X.; Barayavuga, T.; He, X.; Mei, X.; Wang, W.; Jiang, G.; Wang, K. Near-Field Optical Characteristics of Ag Nanoparticle within the Near-Field Scope of a Metallic AFM Tip Irradiated by SNOM Laser. *Integr. Ferroelectr.* **2017**, *178*, 117−124.
(14) Cui, J.; Yang, L.; Xie, H.; Wang, Y.; Mei, X.; Wang, K.; Wang, W.; Hou, C. New Optical Near-Field Nanolithography with Optical

DOI: 10.1021/acsnano.8b05235
ACS Nano 2018, 12, 10703−10711

Fiber Probe Laser Irradiating Atomic Force Microscopy Probe Tip. *Integr. Ferroelectr.* **2016**, *169*, 124−132.
(15) Liu, B. H.; Yang, L. J.; Wang, Y.; Cui, J. L. Particles Nanomanipulation by the Enhanced Evanescent Field through a Near-Field Scanning Optical Microscopy Probe. *Sens. Actuators, A* **2011**, *169*, 171−177.
(16) Chaumet, P.; Rahmani, A.; Nieto-Vesperinas, M. Optical Trapping and Manipulation of Nano-Objects with an Apertureless Probe. *Phys. Rev. Lett.* **2002**, *88*, 123601.
(17) Maragò, O. M.; Jones, P. H.; Gucciardi, P. G.; Volpe, G.; Ferrari, A. C. Optical Trapping and Manipulation of Nanostructures. *Nat. Nanotechnol.* **2013**, *8*, 807−819.
(18) Gao, D.; Ding, W.; Nieto-Vesperinas, M.; Ding, X.; Rahman, M.; Zhang, T.; Lim, C.; Qiu, C. W. Optical Manipulation from the Microscale to the Nanoscale: Fundamentals, Advances, and Prospects. *Light: Sci. Appl.* **2017**, *6*, e17039.
(19) Yan, R.; Park, J. H.; Choi, Y.; Heo, C. J.; Yang, S. M.; Lee, L. P.; Yang, P. Nanowire-Based Single-Cell Endoscopy. *Nat. Nanotechnol.* **2012**, *7*, 191−196.
(20) Singhal, R.; Orynbayeva, Z.; Sundaram, R. V. K.; Niu, J. J.; Bhattacharyya, S.; Vitol, E. A.; Schrlau, M. G.; Papazoglou, E. S.; Friedman, G.; Gogotsi, Y. Multifunctional Carbon-Nanotube Cellular Endoscopes. *Nat. Nanotechnol.* **2011**, *6*, 57−64.
(21) Rios, G.; Lubenov, E. V.; Chi, D.; Roukes, M. L.; Siapas, A. G. Nanofabricated Neural Probes for Dense 3-D Recordings of Brain Activity. *Nano Lett.* **2016**, *16*, 6857−6862.
(22) Gramotnev, D. K.; Bozhevolnyi, S. I. Nanofocusing of Electromagnetic Radiation. *Nat. Photonics* **2014**, *8*, 13−22.
(23) Taminiau, T. H.; Moerland, R. J.; Segerink, F. B.; Kuipers, L.; van Hulst, N. F. $\lambda/4$ Resonance of an Optical Monopole Antenna Probed by Single Molecule Fluorescence. *Nano Lett.* **2007**, *7*, 28−33.
(24) Liang, F.; Zhang, Y.; Hong, W.; Dong, Y.; Xie, Z.; Quan, Q. Direct Tracking of Amyloid and Tau Dynamics in Neuroblastoma Cells Using Nanoplasmonic Fiber Tip Probes. *Nano Lett.* **2016**, *16*, 3989−3994.
(25) Höppener, C.; Novotny, L. Antenna-Based Optical Imaging of Single Ca^{2+} Transmembrane Proteins in Liquids. *Nano Lett.* **2008**, *8*, 642−646.
(26) Shambat, G.; Kothapalli, S. R.; Provine, J.; Sarmiento, T.; Harris, J.; Gambhir, S. S.; Vučković, J. Single-Cell Photonic Nanocavity Probes. *Nano Lett.* **2013**, *13*, 4999−5005.
(27) Schuergers, N.; Lenn, T.; Kampmann, R.; Meissner, M. V.; Esteves, T.; Temerinac-Ott, M.; Korvink, J. G.; Lowe, A. R.; Mullineaux, C. W.; Wilde, A. Cyanobacteria Use Micro-Optics to Sense Light Direction. *eLife* **2016**, *5*, e12620.
(28) Lee, H. J.; Ha, J. H.; Kim, S. G.; Choi, H. K.; Kim, Z. H.; Han, Y. J.; Kim, J.; Oh, Y.; Fragoso, V.; Shin, K.; Hyeon, T.; Choi, H. G.; Oh, K. H.; Baldwin, I. T.; Hyeon, T. Stem-Piped Light Activates Phytochrome B to Trigger Light Responses in *Arabidopsis Thaliana* Roots. *Sci. Signaling* **2016**, *9*, ra106.
(29) Franze, K.; Grosche, J.; Skatchkov, S. N.; Schinkinger, S.; Foja, C.; Schild, D.; Uckermann, O.; Travis, K.; Reichenbach, A.; Guck, J. Müller Cells are Living Optical Fibers in the Vertebrate Retina. *Proc. Natl. Acad. Sci. U. S. A.* **2007**, *104*, 8287−8292.
(30) Olof, S. N.; Grieve, J. A.; Phillips, D. B.; Rosenkranz, H.; Yallop, M. L.; Miles, M. J.; Patil, A. J.; Carberry, D. M. Measuring Nanoscale Forces with Living Probes. *Nano Lett.* **2012**, *12*, 6018−6023.
(31) Phillips, D. B.; Grieve, J. A.; Olof, S. N.; Kocher, S. J.; Bowman, R.; Padgett, M. J.; Miles, M. J.; Carberry, D. M. Surface Imaging Using Holographic Optical Tweezers. *Nanotechnology* **2011**, *22*, 285503.
(32) Miccio, L.; Memmolo, P.; Merola, F.; Netti, P. A.; Ferraro, P. Red Blood Cell as an Adaptive Optofluidic Microlens. *Nat. Commun.* **2015**, *6*, 6502.
(33) Li, Y.; Liu, X.; Yang, X.; Lei, H.; Zhang, Y.; Li, B. Enhancing Upconversion Fluorescence with a Natural Bio-microlens. *ACS Nano* **2017**, *11*, 10672−10680.
(34) Gather, M. C.; Yun, S. H. Single-Cell Biological Lasers. *Nat. Photonics* **2011**, *5*, 406−410.
(35) Xin, H.; Li, Y.; Liu, X.; Li, B. *Escherichia Coli*-Based Biophotonic Waveguides. *Nano Lett.* **2013**, *13*, 3408−3413.
(36) Svoboda, K.; Block, S. M. Biological Applications of Optical Forces. *Annu. Rev. Biophys. Biomol. Struct.* **1994**, *23*, 247−285.
(37) Simpson, S. H.; Zemánek, P.; Maragò, O. M.; Jones, P. H.; Hanna, S. Optical Binding of Nanowires. *Nano Lett.* **2017**, *17*, 3485−3492.
(38) Dholakia, K.; Zemánek, P. Colloquium: Gripped by Light: Optical Binding. *Rev. Mod. Phys.* **2010**, *82*, 1767−1791.
(39) Phillips, D. B.; Carberry, D. M.; Simpson, S. H.; Schäfer, H.; Steinhart, M.; Bowman, R.; Gibson, G. M.; Padgett, M. J.; Hanna, S.; Miles, M. J. Optimizing the Optical Trapping Stiffness of Holographically Trapped Microrods Using High-Speed Video Tracking. *J. Opt.* **2011**, *13*, 044023.
(40) Mariella, R. P.; Huang, Z.; Langlois, R. G. Characterization of the Sensitivity of Side Scatter in a Flow-Stream Waveguide Flow Cytometer. *Cytometry* **1999**, *37*, 160−163.
(41) Darafsheh, A.; Astratov, V. N. Periodically Focused Modes in Chains of Dielectric Spheres. *Appl. Phys. Lett.* **2012**, *100*, 061123.
(42) Kapitonov, A. M.; Astratov, V. N. Observation of Nanojet-Induced Modes with Small Propagation Losses in Chains of Coupled Spherical Cavities. *Opt. Lett.* **2007**, *32*, 409−411.
(43) An, Y.; Chen, M.; Xue, Q.; Liu, W. Preparation and Self-Assembly of Carboxylic Acid-Functionalized Silica. *J. Colloid Interface Sci.* **2007**, *311*, 507−513.
(44) Born, M.; Wolf, E. *Principles of Optics*; Cambridge University Press: 1999.
(45) Khorasaninejad, M.; Chen, W. T.; Devlin, R. C.; Oh, J.; Zhu, A. Y.; Capasso, F. Metalenses at Visible Wavelengths: Diffraction-Limited Focusing and Subwavelength Resolution Imaging. *Science* **2016**, *352*, 1190−1194.
(46) Lee, J. Y.; Hong, B. H.; Kim, W. Y.; Min, S. K.; Kim, Y.; Jouravlev, M. V.; Bose, R.; Kim, K. S.; Hwang, I.-C.; Kaufman, L. J.; Wong, C. W.; Kim, P.; Kim, K. S. Near-Field Focusing and Magnification through Self-Assembled Nanoscale Spherical Lenses. *Nature* **2009**, *460*, 498−501.
(47) Heilemann, M.; Van De Linde, S.; Schüttpelz, M.; Kasper, R.; Seefeldt, B.; Mukherjee, A.; Tinnefeld, P.; Sauer, M. Subdiffraction-Resolution Fluorescence Imaging with Conventional Fluorescent Probes. *Angew. Chem., Int. Ed.* **2008**, *47*, 6172−6176.
(48) Rogers, E. T.; Lindberg, J.; Roy, T.; Savo, S.; Chad, J. E.; Dennis, M. R.; Zheludev, N. I. A Super-Oscillatory Lens Optical Microscope for Subwavelength Imaging. *Nat. Mater.* **2012**, *11*, 432−435.
(49) Conchello, J. A.; Lichtman, J. W. Optical Sectioning Microscopy. *Nat. Methods* **2005**, *2*, 920−931.
(50) Malagnino, N.; Pesce, G.; Sasso, A.; Arimondo, E. Measurements of Trapping Efficiency and Stiffness in Optical Tweezers. *Opt. Commun.* **2002**, *214*, 15−24.
(51) Ashkin, A.; Dziedzic, J. M.; Bjorkholm, J. E.; Chu, S. Observation of a Single-Beam Gradient Force Optical Trap for Dielectric Particles. *Opt. Lett.* **1986**, *11*, 288−290.

DOI: 10.1021/acsnano.8b05235
ACS Nano 2018, 12, 10703−10711